International Journal of Environmental Science and Technology
https://doi.org/10.1007/s13762-024-05602-y

ORIGINAL PAPER

An ingenious investigation on the adsorptive and antibacterial properties of a novel silver-doped hydrochar

Suhas[1] · M. Chaudhary[2] · S. Chaudhary[1] · M. Singh[1] · M. H. Dehghani[3,4] · I. Tyagi[5] · I. P. P. Cansado[6] · S. Kumar[7] · S. Kumar[7]

Received: 10 August 2023 / Revised: 23 December 2023 / Accepted: 10 March 2024

Abstract

A novel silver-doped hydrochar (Ag-HC-230) was synthesized at 230 °C via hydrothermal carbonization of *Tectona grandis* seeds (TGs). The characteristic properties of the Ag-HC-230 were investigated using FTIR, XRD, TGA, SEM and surface area measurements. These results were further utilized for exploring the removal efficiency of the prepared material for chemical and biological contaminants. The surface area and pore volume of Ag-HC-230 were observed to be 24.9 m^2g^{-1} and 0.073 cm^3g^{-1}, respectively. The ultimate analysis demonstrated that the prepared adsorbent was rich in C content (67.77%) as compared to N, H and S content. An ingenious investigation on the antibacterial and adsorptive performance of Ag-HC-230 was evaluated too. The antibacterial performance of Ag-HC-230 was analysed by the agar well diffusion method against the cultured suspensions of *S. aureus* and *E. coli*. To provide a better insight of Ag-HC-230, the removal of acridine yellow G (AYG) was also studied and the experimental removal capacity was found to be 0.073 $mmolg^{-1}$ which was higher than undoped hydrochar HC-230-4 (0.058 $mmolg^{-1}$). The kinetic experimental data were tested by fitting with different kinetics models, and the PSO model was found to be effectively applicable. The adsorption data of AYG on Ag-HC-230 were evaluated using Temkin, Freundlich, Langmuir and D-R among which the data well fitted with the Langmuir model.

Keywords Adsorption · Acridine yellow G · Antibacterial activity · Biological contaminants · Hydrothermal carbonization · Silver doping

Editorial responsibility: S. Mirkia.

✉ Suhas
suhasnatyan@yahoo.com

1 Department of Chemistry, Gurukula Kangri (Deemed to be University), Haridwar 249404, India

2 Department of Chemistry, Hariom Saraswati P.G. College, Dhanauri, Haridwar 247667, India

3 Department of Environmental Health Engineering, School of Public Health, Tehran University of Medical Sciences, Tehran, Iran

4 Center for Solid Waste Research, Institute for Environmental Research, Tehran University of Medical Sciences, Tehran, Iran

5 Centre for DNA Taxonomy, Molecular Systematics Division, Zoological Survey of India, Kolkata 700 053, India

6 Mediterranean Institute for Agriculture, Environment and Development, Chemistry and Biochemistry Department, University of Évora, Rua Romão Ramalho, nº 59, 7000-671 Évora, Portugal

7 Department of Botany and Microbiology, Gurukula Kangri (Deemed to be University), Haridwar 249404, India

Introduction

Modification with metal doping of sustainable carbon materials/chars has emerged as an attractive route to enhance their adsorption potential as well as the antibacterial activities (Trinh et al. 2020; Chandra Joshi et al. 2022). Moreover, the preparation of low-cost, green and sustainable adsorbents (Gupta et al. 2009; Gupta and Suhas 2009; Mei et al. 2023) has become an area of thirst for the researchers in the present scenario. To quench this quest, the biomass proved to be a sustainable and renewable material, which can be easily employed as a precursor for the production of low-cost adsorbents. In order to achieve this, different techniques such as pyrolysis, torrefaction and gasification (Doddapaneni et al. 2017; Zuo et al. 2018; Catizzone et al. 2021) are used worldwide. Recently, a novel green thermochemical process namely hydrothermal carbonization (HTC) which also has been identified as a cost-effective and energy efficient approach for the preparation of the carbon rich materials (hydrochars) has gained tremendous attention (Zhai 2018; Masoumi et al. 2021; Suhas et al. 2021; Suhas et al. 2022). Hydrochar, the resultant

Published online: 03 April 2024

of this process and resembling coal, has been found to be rich in functional groups and carbon contents. It was successfully utilized for the adsorption of a variety of pollutants from water streams (Dai et al. 2021; Ighalo et al. 2022). However, the low surface area and rudimentary porosity of hydrochar limit its adsorptive potential (Zhu et al. 2015).

Modification of hydrochars by introducing the metals can enhance their physical and chemical properties, thereby making them appealing materials for the remediation of broad range of chemical (dyes, phenols, metals, pesticides, insecticides, etc.) as well as biological (bacteria, fungi, viruses, etc.) contaminants. Among these, dyes and bacteria are toxic in nature covering a major part of water pollution (Chaudhary et al. 2021; Valli Nachiyar et al. 2023). Therefore, an urgent attention is needed for their removal. Researchers make continuous efforts to minimize this serious issue as remediation of this precious commodity; water is their primary responsibility.

Based on literature review, it is worth to mention that no work has been reported on the doping of Ag to hydrochar and their application in the removal of dye/bacteria. In present study, we propose a threefold work: (i) embedding silver into hydrochar hereby named as Ag-doped *TGs* derived hydrochar (Ag-HC-230); (ii) characterize the prepared material (Ag-HC-230); (iii) to make an ingenious investigation on the antibacterial and adsorptive performance of Ag-HC-230 by determining its potential for the removal of S. aureus and E.coli bacteria and acridine yellow G (AYG) dye, respectively.

Materials and methods

Materials

AYG dye was procured from Loba Chemie, India, and utilized as adsorbate in the current study. $AgNO_3$ was purchased from Merck, Germany. All other chemicals utilized were of AR grade. *TGs* used as precursor in this study were collected from the trees in the locality of Haridwar. Before any treatment, the seeds were crushed to powdered form, washed with distilled water and oven-dried at 105 °C for 24 h. The sample so prepared was further sieved to obtain a 10–30 mesh size.

Synthesis of materials

The Ag-HC-230 was developed via Co-hydrothermal treatment of TGs and $AgNO_3$ in a 600-ml reactor. For this purpose, 10 g of TGs was mixed with 100 ml distilled water in a teflon lined reactor and 1 ml of 0.1 M $AgNO_3$ was further added and shaken well to homogenize the sample. The reactor was then set to the 230 °C with 4 h residence time and was cooled down to the room temperature on completion of the reaction. The resulting product so obtained was washed, filtered with distilled water and subsequently dried at 105 °C for 24 h to give the final material (Ag-HC-230). The HC-230–4 was prepared same as above but without $AgNO_3$.

Characterization studies

Proximate analysis was done as per American Society for Testing and Materials (ASTM) standards (D3175-07, ASTM D4442-07 and ASTM E1755-01). For this purpose, a muffle furnace (NSW, NSW-101, India) and a temperature programmed oven (NSW, Model- NSW-143, India) was utilized. An elemental analyser (Vario Micro, CHNS analyser, Germany) was utilized for the determination of carbon, hydrogen, sulphur and nitrogen. The surface morphology of Ag-HC-230 was determined by means of SEM (Make-Zeiss, Model- EVO 18 Special Edition, Germany). The crystal structure of Ag-HC-230 was determined using X-ray diffractometer (Make-Rigaku, Japan) with Cu Kα radiation. A method described by Carrott et.al (Carrott et al. 2008) was utilized to determine the pH_{pzc} of the adsorbent (Ag-HC-230). The Fourier transform infrared (FTIR) spectroscopy (Model-Spectrum Two, Make-Perkin Elmer, USA) was used for the surface analysis of Ag-HC-230. The surface area was determined using a surface area analyser (Model-NOVA, Make-Quantachrome, USA). The temperature profile of Ag-HC-230 was determined using thermogravimetric analyser (Model-EXSTAR TG/DTA 6300, Seiko Instruments Inc., Japan).

Adsorption studies

For adsorption studies, batch method was adopted in which a fixed amount of prepared sample, i.e. 10 mg, was added to the 10 ml of AYG at varying concentrations under continuous shaking in a temperature controlled shaking assembly at a fixed temperature for desired time to reach the equilibrium. After the adsorption, the samples were filtrated and the concentrations of AYG were determined by a UV–VIS spectrophotometer (Model-UV-1800, Make-Shimadzu, Japan) at 445 nm wavelength. The pH of all solution in contact with adsorbents was found in the range 8 ± 0.5.

Antibacterial studies

The agar-well diffusion method was applied to determine the preliminary antibacterial activity of Ag-HC-230 and HC-230-4 against standard bacterial strains of Gram-positive bacterium, viz. *S. aureus* (MTCC 740), and Gram-negative bacterium, viz. *E. coli* (MTCC 443) at different concentration of 50, 75 and 100 $mgml^{-1}$. Using sterile cotton swab, 100 µL of bacterial suspension with 0.5 McFarland turbidity standard (1.5×10^8 CFU/ml) of tested bacteria was evenly spread on sterilized MHA plates. Agar wells (6 mm in diameter) were made by using sterile cork-borer. An amount of 100 µL of 50, 75 and 100 $mgmL^{-1}$ of Ag-HC-230

and HC-230-4 was separately added to each well of agar plates. A negative control, i.e. dimethyl sulfoxide (100 µL/well), was separately added to well of agar plates and several standard antibacterial drugs, viz. ampicillin 10 mcg (A), ciprofloxacin 10 mcg (Cf), colistin 10 mcg (Cl), Co-trimoxazole 25 mcg (Co), gentamicin 10 mcg (G), nitrofurantoin 300 mcg (Nf), streptomycin 10 mcg (S) and tetracycline 30 mcg (T) used as positive control against tested bacterial strains. All MHA plates were incubated for 24 h at 37 °C, and the plates were then examined to calculate the zone of inhibition that developed around the individual wells. All assays for determinations of antibacterial potential were carried out in triplicate, and mean value of diameter of bacterial inhibition zone was recorded. The mean and standard deviation of the results were statistically examined using one-way analysis of variance (ANOVA) with P value less than 0.05.

Results and discussion

Characteristics of Ag-HC-230

The volatile, ash and moisture contents of Ag-HC-230 determined in accordance with the ASTM standards were found to be 37.6, 2.7 and 6.8%, respectively. The fixed carbon content was also determined and found to be 52.9%. The ultimate analysis demonstrated that the prepared adsorbent was rich in C content (67.77%) as compared to N, H and S which were found to be 0.07, 5.051 and 0.027%, respectively. The oxygen content in Ag-HC-230 was calculated (by difference) and found to be 24.38%. The value of pH_{pzc} of the Ag-HC-230 was found to be 4.7, demonstrating the surface of Ag-HC-230 to be neutral at this point. The surface of the hydrochar was negatively charged and rich in oxygenated functional groups as reported in previous works (Fang et al. 2015; Takaya et al. 2016). These studies were also confirmed by the FTIR (Fig. 1) by which the functional groups present on the surface of Ag-HC-230 were analysed. The peaks observed at 1512, 1508, 1458, 1211 and 1112 cm^{-1} were owing to presence of ether, carboxylic, ketone and ester groups confirming the presence of oxygenated functional groups on the surface; however, doping of silver limits these groups in comparison with the pure hydrochar indicating that the doping of the silver particles affects the hydrochar matrix (Chandra Joshi et al. 2022). The peaks at 2932 and 516 cm^{-1} were due to the C–H stretching and bending vibrations, respectively. The peak nearly to 3400 cm^{-1} was due to the stretching vibrations of hydroxyl groups. The SEM images (Fig. 2a) explain the morphology of Ag-HC-230 showing the presence of some spherical shaped bright particles on the irregular surface of Ag-HC-230 indicating that the silver was doped into the hydrochar matrix uniformly (Chandra Joshi et al. 2022). Ag-HC-230 analysed by XRD (Fig. 2b) showed intense peaks at 15° (101) and 22.5° (002) indicating that the prepared sample (Ag-HC-230) retained the cellulosic structure post-hydrothermal carbonization and shows the co-existence of amorphous and crystalline structures (Guo et al. 2015; Zhang et al. 2015). The presence of diffraction peaks at 38.48° (200), 44.80° (220), 64.62° (311) confirms the presence of silver in Ag-HC-230. TG-DTG analysis was also performed in order to examine the degradation behaviour and thermal stability of the Ag-HC-230. Three main decomposition stages can be observed from the recorded curves for the analysed sample. TG-DTG

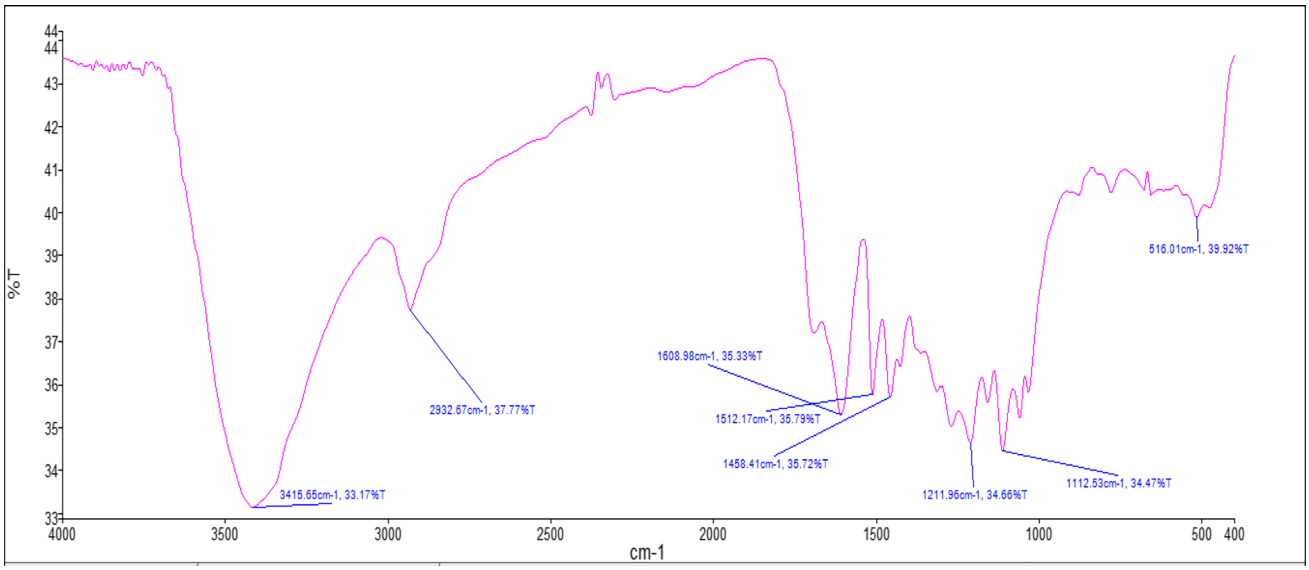

Fig. 1 FTIR spectra of Ag-HC-230

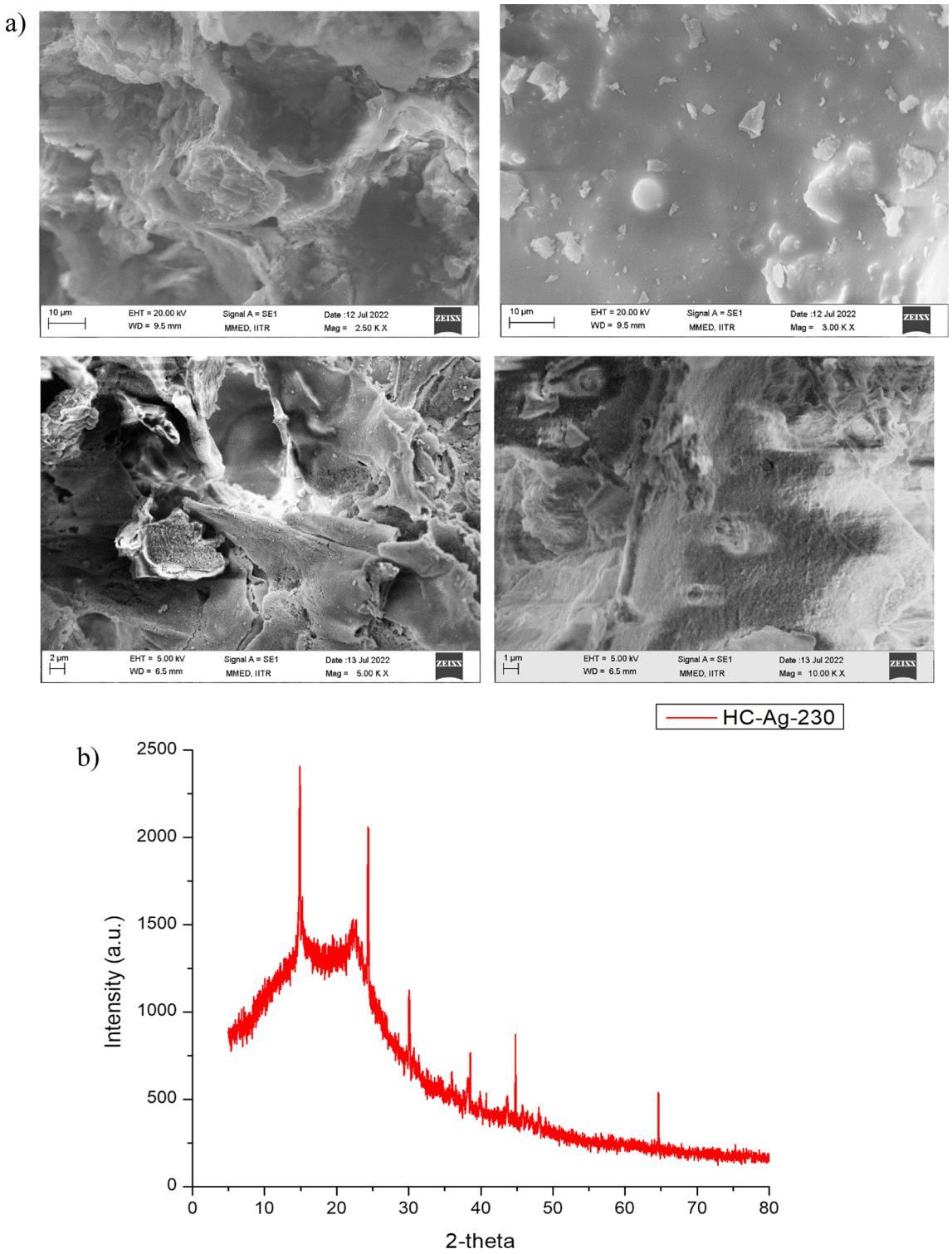

Fig. 2 **a** SEM and **b** XRD of Ag-HC-230

analysis was performed in order to examine the degradation behaviour and thermal stability of the prepared novel silver-doped hydrochar (Ag-HC-230). Three main decomposition stages can be observed from the recorded curves (Fig. 3) for the analysed sample. A slight mass loss, for Ag-HC-230 (2.3%), was observed near 100 °C and can be attributed to the evaporation of unbound and physically sorbed light volatiles and water (Liu et al. 2014). The second stage known

as the pyrolytic zone occurs between 200 and 500 °C with 40% mass loss for Ag-HC-230 and can be attributed to the evaporation of structural waters, cellulose decomposition and devolatilization of hemicellulose and lignin (Shakya et al. 2019). Third, moderate step occurred between 500 and 800 °C with a mass loss of 10.7% which was due to the residual decomposition of lignin and development of carbon structures (Álvarez-Murillo et al. 2015). Therefore, it can be said that the prepared Ag-HC-230 has good thermal stability. The DTG curve for the Ag-HC-230 also showed the change in the thermal ability on HTC. The maximum weight loss rate can be identified by a peak at 349 °C for Ag-HC-230. The high DTG and peak temperature exhibited by Ag-HC-230 suggests a good thermal stability as the temperature at the maximum weight loss is inversely proportional to reactivity (Haykırı-Açma 2003; Islam et al. 2015). The surface area and porosity is an another crucial factor that affects the adsorption capacity of the samples. The surface area and porosity of Ag-HC-230 were measured by means of nitrogen adsorption desorption isotherm. The BET surface area of Ag-HC-230 was found to be 24.9 m^2g^{-1}, and the pore volume and average pore diameter as calculated by BJH method were found to be 0.105 cm^3g^{-1} and 3.6 nm, respectively.

Adsorption studies

Kinetic studies

The kinetic investigations of the adsorption of AYG at a fixed concentration (6×10^{-5} M) onto a fixed amount of Ag-HC-230 for 24 h was examined and compared with HC-230-4. Figure 4 shows the plot of the adsorbed amount versus contact time at two different initial AYG concentrations (5×10^{-5}; 6×10^{-5} M). The adsorption of AYG was quick in the initial time span due to the availability of ample vacant sites on the adsorbent. However, as time progresses, the vacant sites on the adsorbent gradually become occupied by the accumulation of AYG molecules, diminishing the rate of adsorption until reaching equilibrium. The maximum amount of AYG was adsorbed within 1 h, and consequently, equilibrium was reached in 4 h. Therefore, the contact time was kept 5 h for all adsorption studies.

The initial concentration of adsorbates is arguably one of the most influential parameters affecting the adsorption process. Therefore, the effect of the initial dye concentration on equilibrium time was tested at two different AYG concentrations (5×10^{-5}; 6×10^{-5} M) and is shown in Fig. 4. It was observed that an increase in the initial concentration

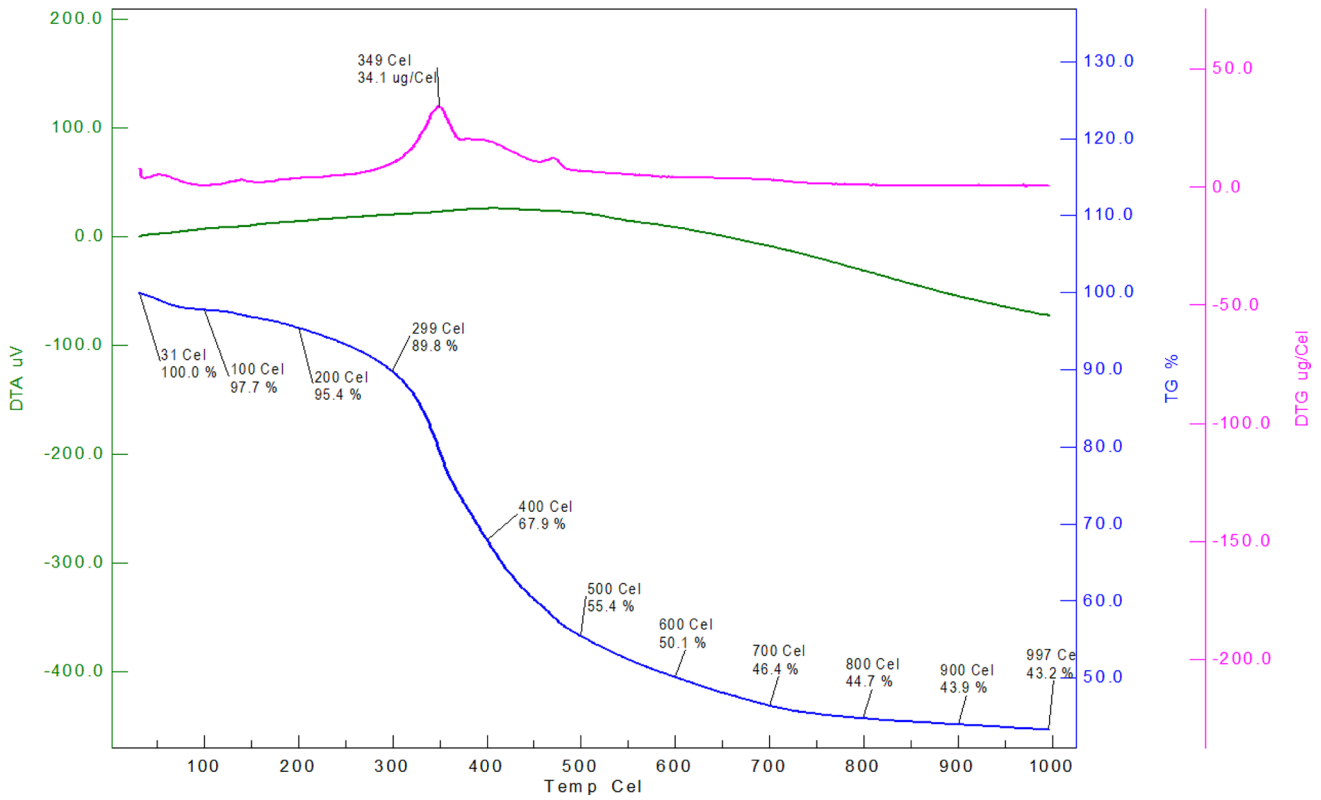

Fig. 3 TGA, DTA and DTG of Ag-HC-230

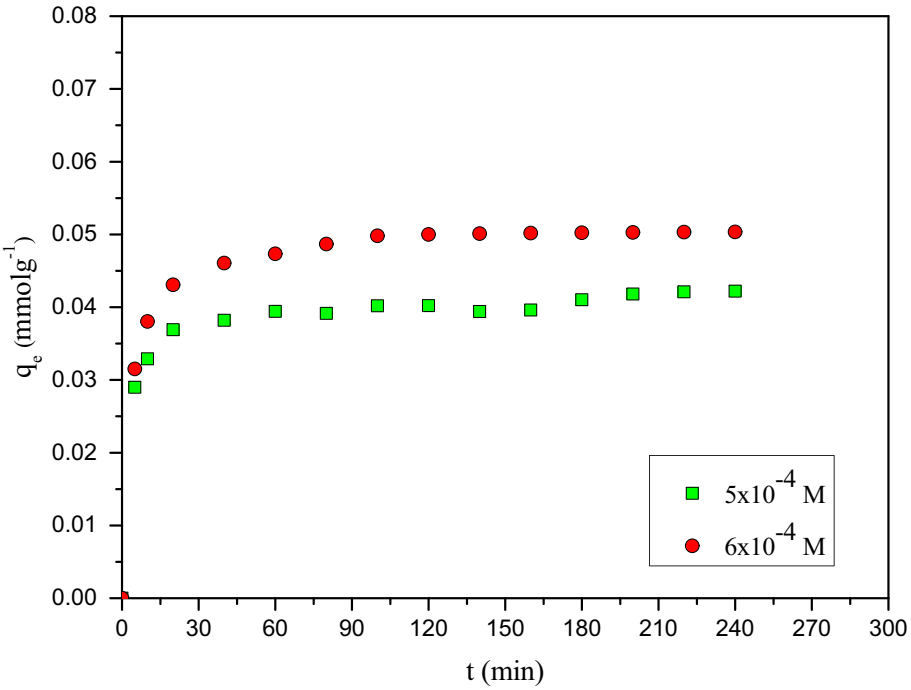

Fig. 4 Effect of contact time and initial concentration on adsorption of AYG onto Ag-HC-230

of AYG is directly correlated with a rise in the adsorption capacity of the Ag-HC-230. It may be attributed to an increase in the driving force due to the concentration gradient on increasing the initial concentration in order to beat the resistance to the mass transfer of dyes between the liquid and solid phases. (Aksu and Akın 2010). Further, the kinetic experimental data were tested by fitting with pseudo-first-order (PFO) (Lagergren 1898), pseudo-second-order (PSO) (Ho and McKay 1998) and Elovich (1959) to investigate the kinetics, and the equations used are as follows:

$$\text{PFO} \quad \log(q_e - q_t) = \log q_e - \frac{k_1}{2.303} t \tag{1}$$

$$\text{PSO} \quad \frac{t}{q_t} = \frac{1}{k_2 q_e^2} + \frac{1}{q_e} t \tag{2}$$

$$\text{Elovich} \quad q_t = 1/\beta \ \ln(\alpha\beta) + 1/\beta \ \ln(t) \tag{3}$$

where q_e and q_t are the amount of AYG adsorbed at equilibrium and time t, respectively. k_1, and k_2 are the rate constants for the PFO and PSO models, respectively. β (gmmol^{-1}) and α (mmolg^{-1} min^{-1}) are the rate constant for desorption and a constant, representing the adsorption of AYG initially on Ag-HC-230, respectively.

The graphs of PFO, PSO and Elovich models for the removal of AYG on HC-230-4 and Ag-HC-230 are shown in Fig. 5a–c, and the obtained kinetic parameters are listed in Table 1. To know the best fitted model, the theoretically calculated values and correlation coefficient (R^2) were taken into consideration. Table 1 shows that the PSO model was effectively applicable on the adsorption data as compared to other model, in terms of the higher values of R^2 and close agreement between experimental and theoretically calculated q_e values.

Effect of pH

The pH of the adsorbate solutions significantly affects the removal efficiency of the adsorbents. Therefore, the developed silver-doped hydrochar (Ag-HC-230) was also tested for its ability to remove AYG dye at varying solution pH (Fig. 6). The amount adsorbed increased on increasing the pH of dye solution. At lower pH (2–4.7), the concentration of H^+ was higher, which competes with AYG for available sites on Ag-HC-230. Therefore, low adsorption capacity was observed in this pH range. Moreover, the surface of Ag-HC-230 is positively charged at pH below 4.7 (pHpzc =4.7) which causes electrostatic repulsion between the positively charged adsorbent and dye cations, resulting in lower adsorption. On the other hand, at pH levels above 5, the surface of Ag-HC-230 is negatively charged and undergoes electrostatic interactions with positively charged dye, resulting in enhanced adsorption at higher pH. The maximum adsorption of AYG is observed between pH 5–8 which was due to deprotonation and electrostatic interactions. Beyond pH 8, a decrease in the adsorption of AYG is observed which is possibly due to the dimerization of dye molecules (Feng and Shi 2007; da Silva Lacerda et al. 2015).

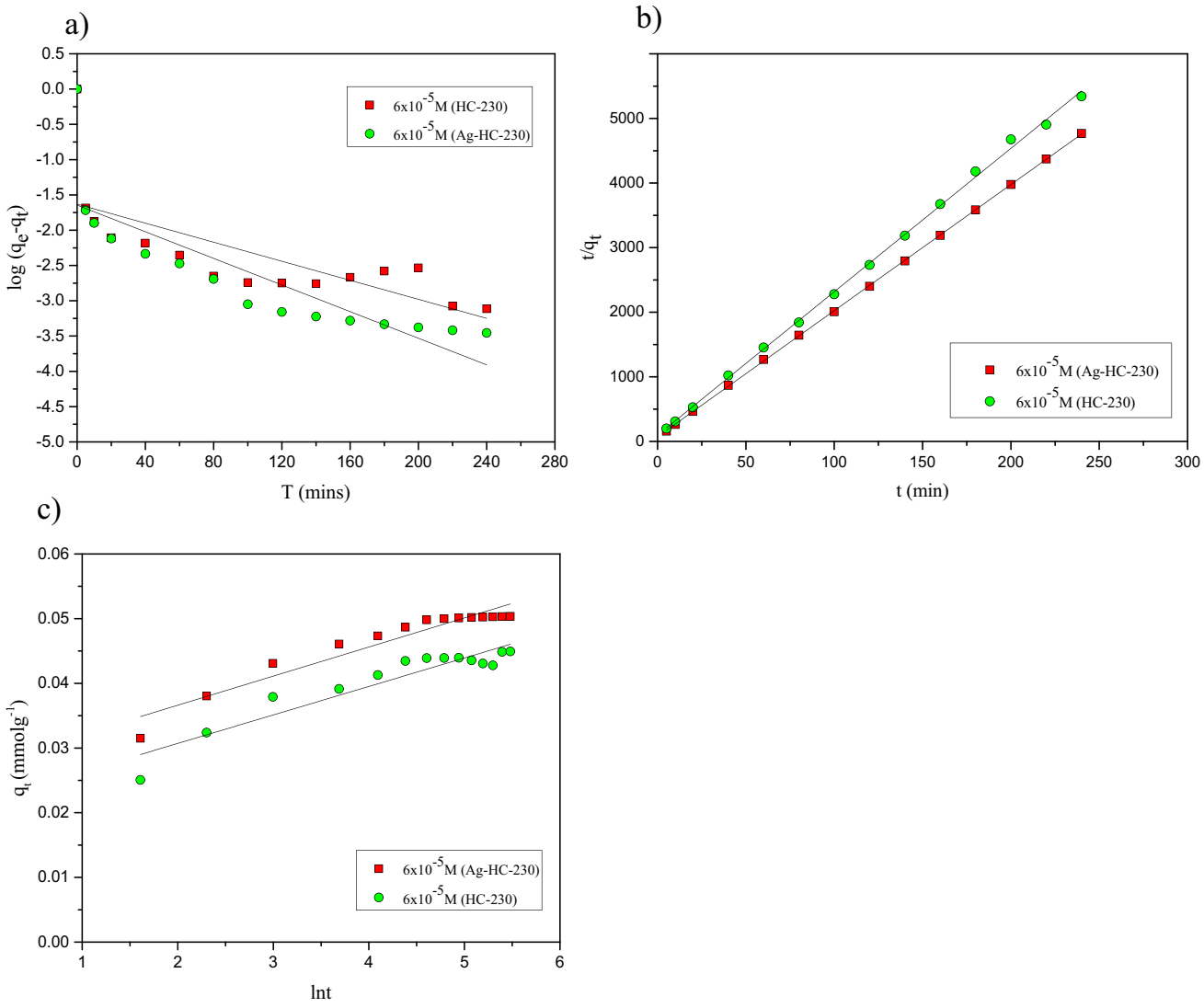

Fig. 5 **a** PFO; **b** PSO; and **c** Elovich model for the adsorption of AYG on Ag-HC-230 and HC-230-4 (Temp: 25 °C; 6×10^{-5} M)

Adsorption isotherms

To determine the mechanism of the adsorption and to understand the type of interaction between the AYG and Ag-HC-230/HC-230-4, isotherm curves were plotted at 25, 35 and 45 °C (Fig. 7). For both materials, an increase in the adsorption of AYG was seen as the initial concentration of dye increased which was possibly due to the increase in driving force of a concentration gradient. The experimental removal capacity (Fig. 7) was found to be 0.089 and 0.058 mmolg^{-1} on Ag-HC-230 and HC-230-4, respectively, for AYG which was found to be higher in case of Ag-HC-230. The behaviour of the adsorption capacity relative to the temperature was also studied, and an increment in the adsorption capacity was seen with increasing the temperature from 25 to 45 °C in both cases, which is indicative of endothermic nature of the process. Based on the experimental results, the adsorption capacity of Ag-HC-230 was quantitatively evaluated by isotherm models, viz. Langmuir (Langmuir 1918), Freundlich (Freundlich 1906), Temkin (Temkin 1940) and D-R (Dubinin 1947). The plots of these models and obtained data are presented in Fig. 8a–d and Table 2, respectively. These models can be represented mathematically as follows:

$$\text{Langmuir} \quad \frac{1}{q_e} = \frac{1}{q_{max}} + \frac{1}{q_{max} b C_e} \tag{4}$$

$$\text{Freundlich} \quad \log q_e = \log K_f + \frac{1}{n} \log C_e \tag{5}$$

$$\text{Temkin} \quad q_e = B_T \ln K_T + B_T \ln C_e \tag{6}$$

Table 1 Kinetic parameters for the removal of AYG on Ag-HC-230 and HC-230-4 at same concentration

Parameters	Ag-HC-230	HC-230-4
C_o (molL^{-1})	6×10^{-5}	6×10^{-5}
$q_{e\ (exp)}$ (mmolg^{-1})	0.0507	0.0457
Pseudo-first order		
$q_{e\ (cal)}$(mmolg^{-1})	0.0097	0.010
K_1 (min^{-1})	1.66×10^{-2}	1.04×10^{-2}
R^2	0.894	0.747
Pseudo-second order		
$q_{e\ (cal)}$ (mmolg^{-1})	0.0512	0.0450
K_2 (g.mmol^{-1}.min^{-1})	5.28	5.10
R^2	0.999	0.998
Elovich		
α (mmolg^{-1}.min^{-1})	2.08	0.638
β (g.mmol^{-1})	222	227
R^2	0.920	0.888

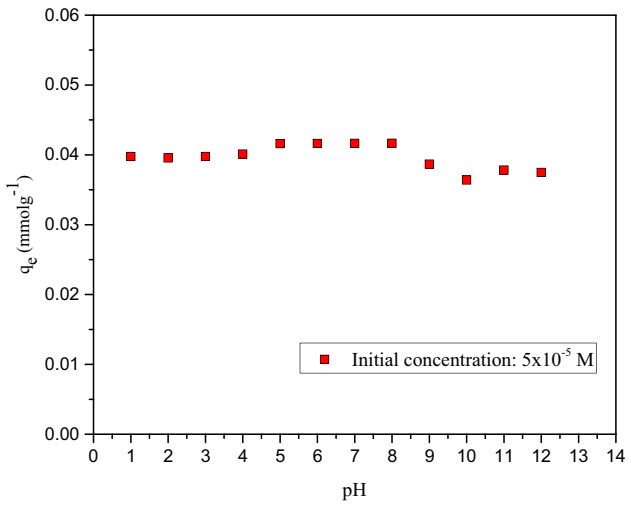

Fig. 6 Effect of pH on the adsorption of AYG onto Ag-HC-230 (C_i: 5×10^{-5} M; T: 25 °C)

$$D-R \qquad \ln\ qe = \ln qm - \beta DR\varepsilon^2 \tag{7}$$

where q_e and C_e are the maximum adsorption capacity of the Ag-HC-230 and concentration of the AYG at equilibrium, respectively, whereas q_{max} is the Langmuir adsorption capacity. The b, K_f, K_T and β are the equilibrium constants for Langmuir, Freundlich, Temkin and D-R models, respectively. Analysing the data by the above models, the adsorption characteristics of Ag-HC-230 were found to be most accurately predicted by Langmuir isotherm model in comparison with the other models owing to the highest co-relation coefficient values and close agreement with the experimental values (Table 2).

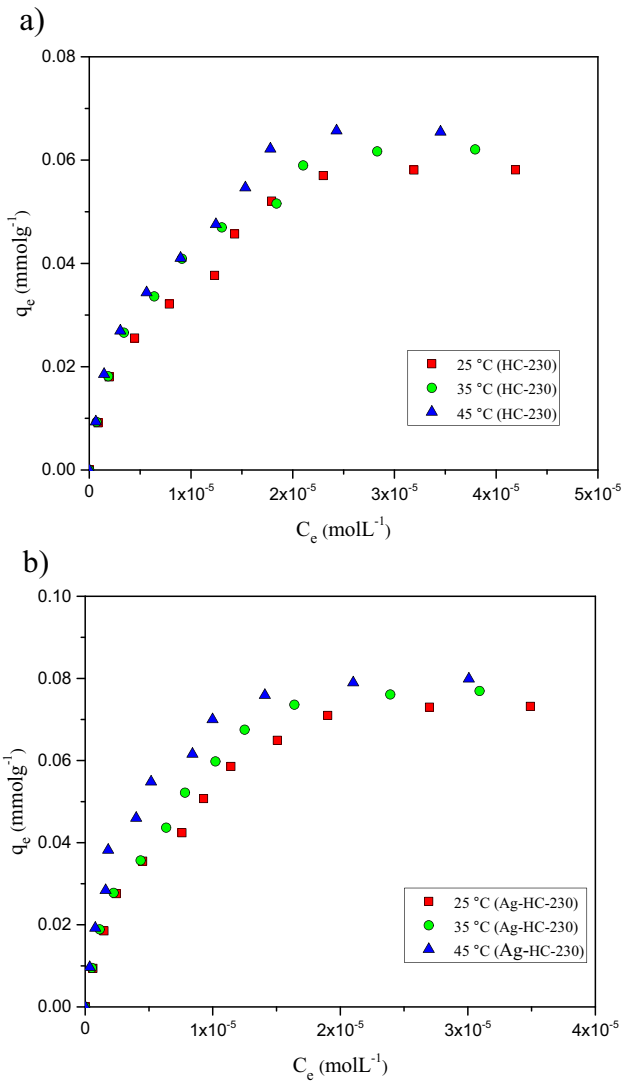

Fig. 7 Adsorption isotherm of AYG on **a** HC-230-4 and **b** Ag-HC-230 at different temperatures

Mechanism of adsorption

The adsorption mechanism of AYG over Ag-HC-230 was governed by various factors, viz. functional groups present on Ag-HC-230, surface area and surface charge on Ag-HC-230. Ag-HC-230 as compared to HC-230-4 adsorb more which can be seen from increased adsorption values which is probably due to enhance surface area (24.9 m^{2}g^{-1}) of Ag-HC-230, the adsorption herein is mainly governed by the interactions between AYG and Ag-HC-230. The surfaces of prepared Ag-HC-230 have oxygenated functional groups which causes surface complexation via electrostatic interactions. Additionally, strong H-bonding between the AYG and Ag-HC-230 results in enhanced adsorption. As the pHpzc of the adsorbent is 4.7 and AYG is a cationic dye, strong electrostatic interactions between them were also contributed to the

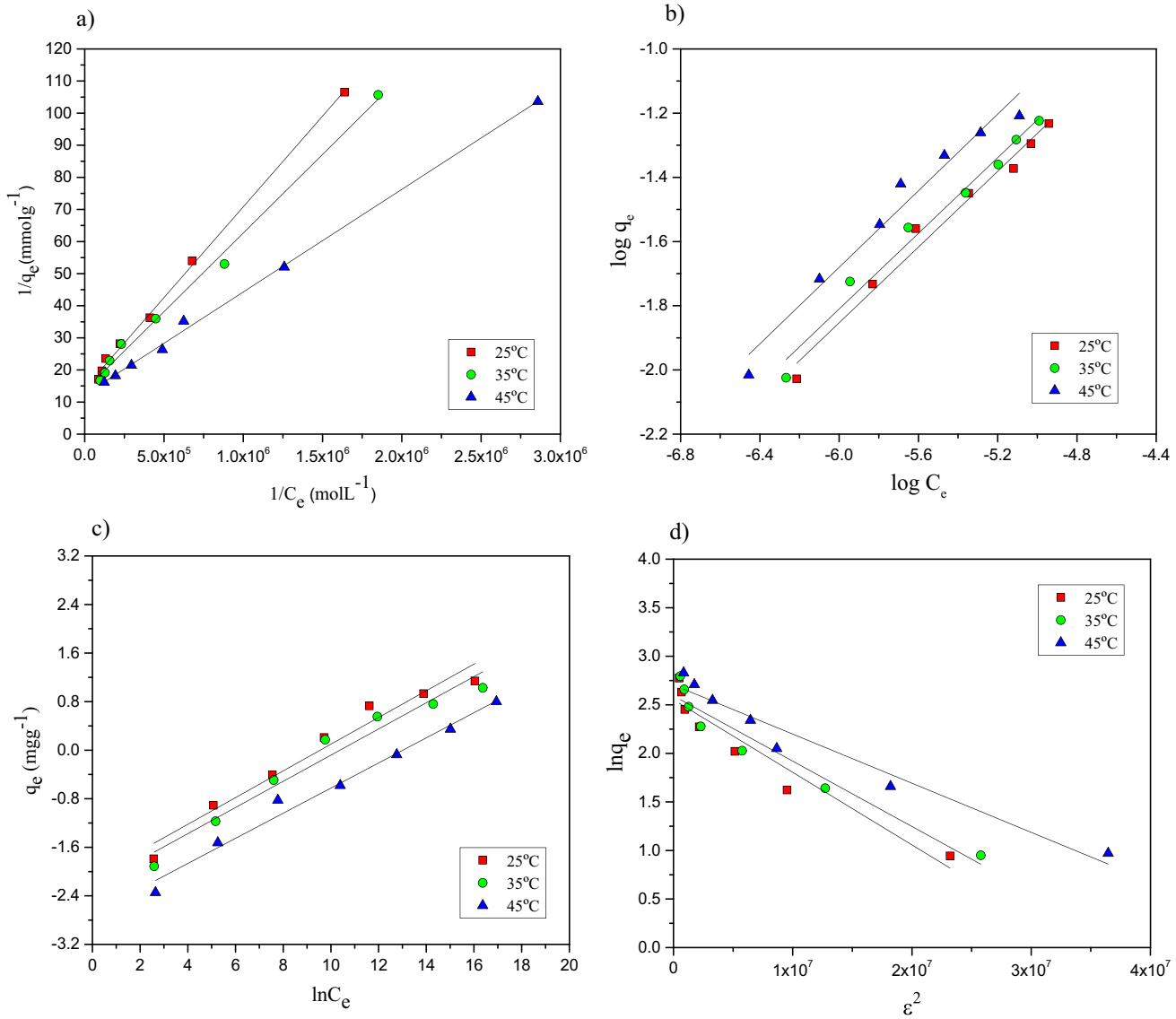

Fig. 8 **a** Langmuir; **b** Freundlich; **c** Temkin and **d** D-R model for adsorption of AYG on Ag-HC-230 at different temperature

adsorption in a positive way. Besides it, the Ag present at the Ag-HC-230 surface may be valuable for the adsorption due to the π–π interactions with the AYG molecules (Aboelfetoh et al. 2020; Louis et al. 2020; Shaikh et al. 2021). Therefore, the electrostatic interactions, hydrogen bonding and π–π stacking governed the adsorption of AYG on Ag-HC-230.

Antibacterial properties of Ag-HC-230

The antibacterial performance of Ag-HC-230 (50, 75 and 100 $mgml^{-1}$) was evaluated by agar well plate diffusion method against the cultured suspensions of Gram-positive bacteria (*S. aureus*) and Gram-negative (*E. coli*) and is presented in Fig. 9 and Table 3. Interestingly, experiments show that the growth of both bacteria inhibited with inhibition zone of 17.33 and 16.33 mm for *S. aureus* and *E. coli*, respectively, when the discs were impregnated with Ag-HC-230 at 100 $mgml^{-1}$ inhibitory concentration. The antibacterial potential of the HC-230-4 prepared at the same conditions without silver doping was tested too, and no inhibitory effect for both the bacteria was observed (Fig. 9; Table 3). This demonstrates that the doping of the silver enhanced the antibacterial properties of the hydrochar. It is well known that $AgNO_3$ shows antibacterial activity; therefore, the prepared material doped with silver (Ag-HC-230) can be used as an antibacterial agent for the studied bacteria. The antibacterial activity was also compared with antibacterial agents such as Streptomycin and Gentamicin as a positive control. The antibacterial effect of these drugs was found to be comparable with Ag-HC-230 against *E. coli* and *S. aureus* and is

Table 2 Different isothermal data for the adsorption of AYG on Ag-HC-230 and HC-230-4

Parameters	Ag-HC-230			HC-230-4		
Temperature (°C)	25	35	45	25	35	45
Experimental data						
q_{exp} (mmolg^{-1})	0.073	0.076	0.080	0.058	0.062	0.066
q_{exp} (mgg^{-1})	19.9	20.8	21.9	15.8	16.9	18.0
Langmuir						
q_{max} (mmolg^{-1})	0.069	0.072	0.082	0.054	0.057	0.061
q_{max} (mgg^{-1})	19.1	19.6	22.5	14.9	15.6	16.7
b (L/mmol)	2.53×10^5	2.90×10^5	3.76×10^5	2.35×10^5	2.66×10^5	2.73×10^5
R^2	0.998	0.995	0.995	0.992	0.997	0.996
Freundlich						
K_f (mmolg^{-1}) (molL^{-1})$^{1/n}$	48.5	51.4	62.9	16.7	17.8	18.7
n	1.70	1.71	1.73	1.89	1.90	1.91
R^2	0.981	0.982	0.951	0.979	0.980	0.975
Temkin						
b (KJmol^{-1})	0.567	0.559	0.536	0.692	0.677	0.661
A_T (Lmg^{-1})	8.89	10.4	15.9	7.14	8.50	9.53
R^2	0.962	0.959	0.977	0.943	0.987	0.978
D-R						
E (KJmol^{-1})	2.59	2.75	3.13	2.31	2.47	2.55
q_m (mgg^{-1})	12.8	13.3	14.9	10.9	11.4	12.0
R^2	0.926	0.938	0.959	0.968	0.949	0.979

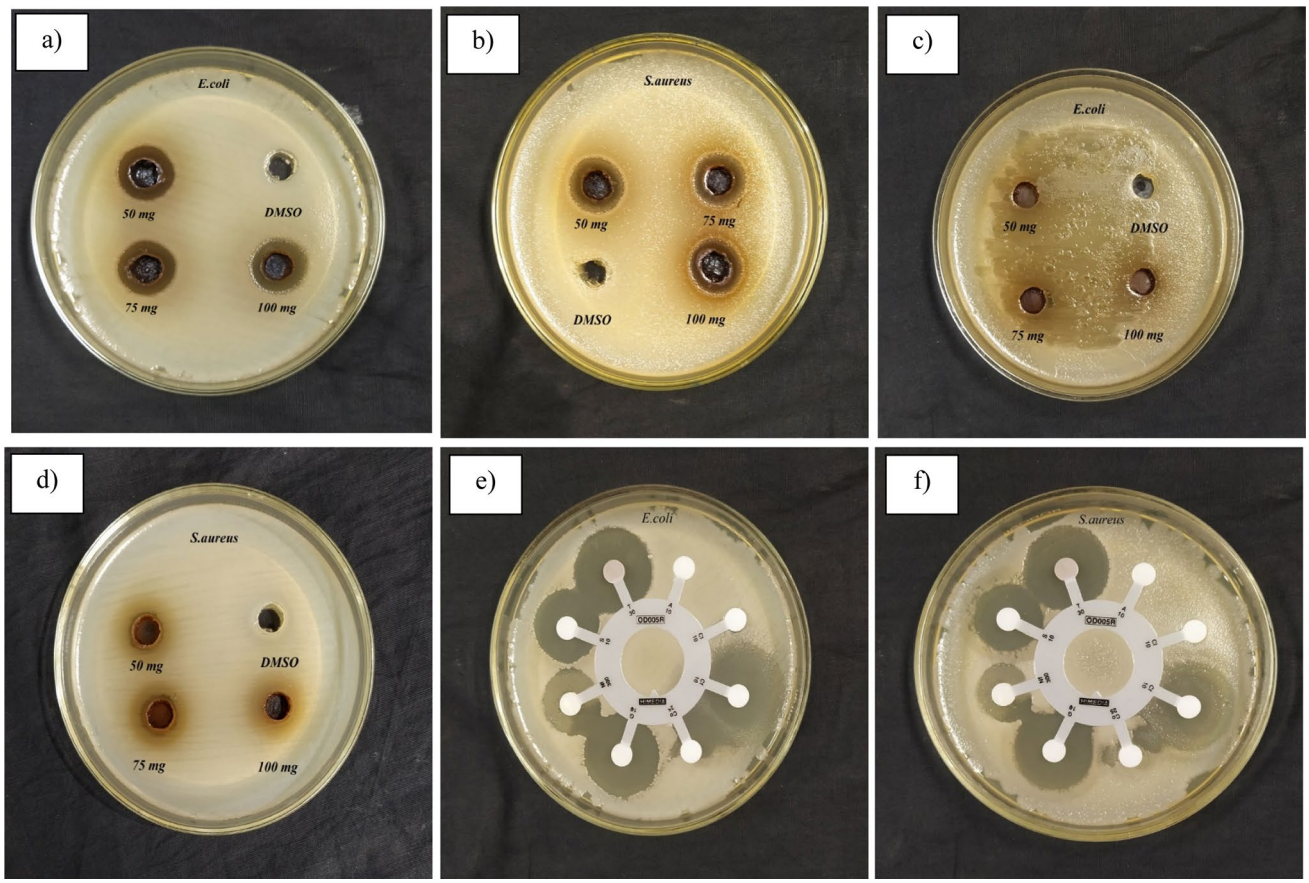

Fig.9 Inhibition zones of *E. coli* and *S. aureus* against HC-Ag-230 **a**–**b**; HC-230-4 **c**–**d**; positive control **e**–**f**

Table 3 Antibacterial activity of Ag-HC-230 and HC-230-4 sample against Gram-negative and Gram-positive bacteria with mean value ± standard error

Sample	Concentration (mg/ml)	Diameter of zone of inhibition (mm)	
		Bacterial strains	
		E.coli	*S. aureus*
HC-Ag-230	50	14.33 ± 0.58	15.33 ± 0.58
	75	15.33 ± 0.58	16.33 ± 0.58
	100	16.33 ± 1.15	17.33 ± 0.58
HC-230-4	50	–	–
	75	–	–
	100	–	–

Table 4 Activity of different antibiotics (positive control) against Gram-negative and Gram-positive bacteria with mean value ± standard deviation

Antibiotics(Positive control)	Diameter of zone of inhibition (mm)	
	Bacterial strains	
	E. coli	*S. aureus*
Ampicillin (A)	–	–
Ciprofloxacin (Cf)	–	–
Colistin (Cl)	27.66 ± 0.58	25.33 ± 0.58
Co-trimoxazole (Co)	–	–
Gentamicin (G)	22.33 ± 0.58	22.66 ± 1.15
Nitrofurantoin (Nf)	17.66 ± 0.58	15.33 ± 0.58
Streptomycin (S)	19.33 ± 0.58	18.33 ± 0.58
Tetracycline (T)	23.33 ± 0.58	21.66 ± 0.58

presented in Table 4 and Fig. 9. The mechanism behind the destruction of the bacterial cell wall by Ag-HC-230 can be observed owing to the electrostatic interactions between the Ag-HC-230 and the modelled bacteria. Firstly, the silver in Ag-HC-230 stuck to the cell wall of bacteria and starts to permeate through the cell membrane, i.e. disrupting the respiratory functions that caused the bacterial death finally. Moreover, cell-wall membrane disruption enhances due to leakage of the cellular components, viz. DNA to the environment that finally lead to the death of the modelled bacteria (Dadi et al. 2019). A comparison with the other antibiotics was also made, and results are presented in Table 4 which shows that the Ag-HC-230 is effective and comparable.

Conclusion

A novel silver-doped *TGs*-derived hydrochar (Ag-HC-230) was prepared and characterized using proximate/ultimate analysis, FTIR, XRD, TGA, SEM and the surface area analysis. Ag-HC-230 was utilized for the removal of dye (AYG) as well as for the antibacterial potential (*S. aureus* and *E.coli*). The electrostatic interactions, hydrogen bonding and π–π stacking governed the adsorption of AYG on Ag-HC-230. The better fit of PSO model in comparison with PFO model, in terms of the higher R^2 values and close agreement between experimental and theoretically calculated qe values, indicated that the PSO model can better explain the removal of AYG on Ag-HC-230. The adsorption characteristics of Ag-HC-230 were found to be most accurately predicted by Langmuir isotherm model in comparison with the other analysed models with the highest co-relation coefficient values. The adsorption of AYG on Ag-HC-230 was also compared with HC-230 at different temperature which signified Ag-HC-230 to be a better adsorbent. The antibacterial activity of silver-doped hydrochar further adds to its value and makes it a pollutant removing versatile material.

Acknowledgment Authors are thankful to DST, New Delhi, India, for the financial support under Water Technology Initiative (Project No: DST/TMD/EWO/WTI/2K19/EWFH/2019/90).

Author contributions S, SC and MC were involved in the conceptualization; S, SC and MC contributed to the methodology, software and validation; S, SC, SK2 and MC were involved in the formal analysis; S, SC and MC performed the investigation; S, SC, SK1 and MC contributed to the resources; S, SC, SK2 and MC curated the data; S, SC and MC contributed to writing—original draft; S, SC, SK1, IT, MHD, MS, IPPC and MC contributed to writing—review and editing; S, SC, IT, IPPC, MHD and MC performed the visualization; S contributed to the supervision. All authors commented on previous versions of the manuscript. All authors read and approved the final manuscript.

Data availability Not applicable.

Declarations

Conflict of interest The authors declare that they have no competing interests.

Ethical approval Not applicable.

Consent to participate Not applicable.

Consent to publication All authors have consented to publish the article.

References

Aboelfetoh EF, Gemeay AH, El-Sharkawy RG (2020) Effective disposal of methylene blue using green immobilized silver nanoparticles on graphene oxide and reduced graphene oxide sheets through one-pot synthesis. Environ Monit Assess 192(6):355. https://doi.org/10.1007/s10661-020-08278-2

Aksu Z, Akın AB (2010) Comparison of remazol black b biosorptive properties of live and treated activated sludge. Chem Eng J 165(1):184–193. https://doi.org/10.1016/j.cej.2010.09.014

Álvarez-Murillo A et al (2015) Study of variables in energy densification of olive stone by hydrothermal carbonization. J Anal Appl Pyrol 113:307–314. https://doi.org/10.1016/j.jaap.2015.01.031

Carrott PJM et al (2008) Characterisation of surface ionisation and adsorption of phenol and 4-nitrophenol on non-porous carbon

blacks. Ads Sci Technol 26(10):827–841. https://doi.org/10.1260/026361708788708252
Catizzone E et al (2021) Purification of wastewater from biomass-derived syngas scrubber using biochar and activated carbons. Int J Environ Res Public Health 18(8):4247
Chandra Joshi H et al (2022) Silver-doped active carbon spheres and their application for microbial decontamination of water. Heliyon 8(4):e09209. https://doi.org/10.1016/j.heliyon.2022.e09209
Chaudhary M et al (2021) Microporous activated carbon as adsorbent for the removal of noxious anthraquinone acid dyes: Role of adsorbate functionalization. J Environ Chem Eng 9(5):106308. https://doi.org/10.1016/j.jece.2021.106308
da Silva LV et al (2015) Rhodamine b removal with activated carbons obtained from lignocellulosic waste. J Environ Manage 155:67–76. https://doi.org/10.1016/j.jenvman.2015.03.007
Dadi R et al (2019) Antibacterial activity of zno and cuo nanoparticles against gram positive and gram negative strains. Mater Sci Eng C 104:109968. https://doi.org/10.1016/j.msec.2019.109968
Dai L et al (2021) Tuning oxygenated functional groups on biochar for water pollution control: a critical review. J Hazard Mater 420:126547. https://doi.org/10.1016/j.jhazmat.2021.126547
Doddapaneni TRKC et al (2017) Adsorption of furfural from torrefaction condensate using torrefied biomass. Chem Eng J. https://doi.org/10.1016/j.cej.2017.10.053
Dubinin MM (1947) The equation of the characteristic curve of activated charcoal. InDokl Akad Nauk SSSR 55:327–329
Elovich S, (1959) Proceedings of the second international congress on surface activity. In: Proceedings of Teh Second International Congress on Surface Activity. Academic Press Inc. New York
Fang J et al (2015) Hydrochars derived from plant biomass under various conditions: characterization and potential applications and impacts. Chem Eng J 267:253–259. https://doi.org/10.1016/j.cej.2015.01.026
Feng S, Shi H (2007) Spectroscopic study on the interaction of acridine yellow with adenosine disodium triphosphate and its analytical application. Spectrochim Acta a Mol Biomol Spectroscopy 68(2):244–249. https://doi.org/10.1016/j.saa.2006.11.022
Freundlich H (1906) Over the adsorption in solution. J Phys Chem 57(385471):1100–1107
Guo S et al (2015) Characteristic evolution of hydrochar from hydrothermal carbonization of corn stalk. J Anal Appl Pyrol 116:1–9. https://doi.org/10.1016/j.jaap.2015.10.015
Gupta VK, Suhas (2009) Application of low-cost adsorbents for dye removal—a review. J Environ Manage 90(8):2313–2342. https://doi.org/10.1016/j.jenvman.2008.11.017
Gupta VK et al (2009) Low-cost adsorbents: growing approach to wastewater treatment—a review. Crit Rev Environ Sci Technol 39(10):783–842. https://doi.org/10.1080/10643380801977610
Haykırı-Açma H (2003) Combustion characteristics of different biomass materials. Ener Convers Manage 44(1):155–162. https://doi.org/10.1016/S0196-8904(01)00200-X
Ho Y-S, McKay G (1998) Sorption of dye from aqueous solution by peat. Chem Eng J 70(2):115–124. https://doi.org/10.1016/S0923-0467(98)00076-1
Ighalo JO et al (2022) Recent advances in hydrochar application for the adsorptive removal of wastewater pollutants. Chem Eng Res Des 184:419–456. https://doi.org/10.1016/j.cherd.2022.06.028
Islam MA et al (2015) Combustion kinetics of hydrochar produced from hydrothermal carbonisation of Karanj (*Pongamia pinnata*) fruit hulls via thermogravimetric analysis. Bioresour Technol 194:14–20. https://doi.org/10.1016/j.biortech.2015.06.094
Lagergren SK (1898) About the theory of so-called adsorption of soluble substances. Sven Vetenskapsakad Handingarl 24:1–39
Langmuir I (1918) The adsorption of gases on plane surfaces of glass, mica and platinum. J Am Chem Soc 40(9):1361–1403. https://doi.org/10.1021/ja02242a004
Liu S et al (2014) Adsorption of the anionic dye congo red from aqueous solution onto natural zeolites modified with n, n-dimethyl dehydroabietylamine oxide. Chem Eng J 248:135–144. https://doi.org/10.1016/j.cej.2014.03.026
Louis MR et al (2020) Silver-loaded biomass (delonix regia) with antibacterial properties as porous carbon composite towards comprehensive water purification. Int J Environ Sci Technol 17(4):2415–2432. https://doi.org/10.1007/s13762-019-02528-8
Masoumi S et al (2021) Hydrochar: a review on its production technologies and applications. Catalysts 11(8):939. https://doi.org/10.3390/catal11080939
Mei M et al (2023) Amino-functionalization of lignocellulosic biopolymer to be used as a green and sustainable adsorbent for anionic contaminant removal. Int J Biol Macromol 227:1271–1281. https://doi.org/10.1016/j.ijbiomac.2022.11.322
Shaikh WA, Islam RU, Chakraborty S (2021) Stable silver nanoparticle doped mesoporous biochar-based nanocomposite for efficient removal of toxic dyes. J Environ Chem Eng 9(1):104982. https://doi.org/10.1016/j.jece.2020.104982
Shakya A, Núñez-Delgado A, Agarwal T (2019) Biochar synthesis from sweet lime peel for hexavalent chromium remediation from aqueous solution. J Environ Manage 251:109570. https://doi.org/10.1016/j.jenvman.2019.109570
Suhas et al (2021) A novel approach to develop activated carbon by an ingenious hydrothermal treatment methodology using phyllanthus emblica fruit stone. J Clean Prod 288:125643. https://doi.org/10.1016/j.jclepro.2020.125643
Suhas et al (2022) Chapter 9—novel hydrochar as low-cost alternative adsorbent for the removal of noxious impurities from water. In: TyagiJ I, Goscianska M, Dehghani H, Karri RR (eds) Sustainable materials for sensing and remediation of noxious pollutants. Elsevier, Amsterdam, pp 149–160
Takaya CA et al (2016) Phosphate and ammonium sorption capacity of biochar and hydrochar from different wastes. Chemosphere 145:518–527. https://doi.org/10.1016/j.chemosphere.2015.11.052
Temkin M (1940) Kinetics of ammonia synthesis on promoted iron catalysts. Acta Physiochim URSS 12:327–356
Trinh VT et al (2020) Phosphate adsorption by silver nanoparticles-loaded activated carbon derived from tea residue. Sci Rep 10(1):3634. https://doi.org/10.1038/s41598-020-60542-0
ValliNachiyar C et al (2023) Developments in treatment technologies of dye-containing effluent: a review. Case Stud Chem Environ Eng 7:100339. https://doi.org/10.1016/j.cscee.2023.100339
Zhai Y (2018) A review of the hydrothermal carbonization of biomass waste for hydrochar formation: process conditions, fundamentals, and physicochemical properties. Renew Sust Energ Rev 90:223–247. https://doi.org/10.1016/j.rser.2018.03.071
Zhang L et al (2015) Hydrothermal carbonization of corncob residues for hydrochar production. Energ Fuels 29(2):872–876. https://doi.org/10.1021/ef502462p
Zhu X et al (2015) Role of hydrochar properties on the porosity of hydrochar-based porous carbon for their sustainable application. ACS Sustain Chem Eng 3(5):833–840. https://doi.org/10.1021/acssuschemeng.5b00153
Zuo W et al (2018) Low-cost and efficient adsorbent derived from pyrolysis of jatropha curcas seeds for the removal of cu^{2+} from aqueous solutions. Chem Ecol 34(7):655–674. https://doi.org/10.1080/02757540.2018.1472246